
On the Identifiability and Interpretability of Gaussian Process Models

Jiawen Chen

Department of Biostatistics
University of North Carolina at Chapel Hill
jiawenn@email.unc.edu

Wancen Mu

Department of Biostatistics
University of North Carolina at Chapel Hill
wancen@live.unc.edu

Yun Li

Department of Biostatistics
University of North Carolina at Chapel Hill
yun_li@med.unc.edu

Didong Li

Department of Biostatistics
University of North Carolina at Chapel Hill
didongli@unc.edu

Abstract

In this paper, we critically examine the prevalent practice of using additive mixtures of Matérn kernels in single-output Gaussian process (GP) models and explore the properties of multiplicative mixtures of Matérn kernels for multi-output GP models. For the single-output case, we derive a series of theoretical results showing that the smoothness of a mixture of Matérn kernels is determined by the least smooth component and that a GP with such a kernel is effectively equivalent to the least smooth kernel component. Furthermore, we demonstrate that none of the mixing weights or parameters within individual kernel components are identifiable. We then turn our attention to multi-output GP models and analyze the identifiability of the covariance matrix A in the multiplicative kernel $K(x, y) = AK_0(x, y)$, where K_0 is a standard single output kernel such as Matérn. We show that A is identifiable up to a multiplicative constant, suggesting that multiplicative mixtures are well suited for multi-output tasks. Our findings are supported by extensive simulations and real applications for both single- and multi-output settings. This work provides insight into kernel selection and interpretation for GP models, emphasizing the importance of choosing appropriate kernel structures for different tasks.

1 Introduction

Gaussian processes (GPs) have emerged as a powerful and popular tool in machine learning, spatial statistics, functional data analysis, etc., due to their versatility, flexibility, and interpretability as a nonparametric method (Rasmussen and Williams, 2006; Banerjee et al., 2014). GPs provide an intuitive means of modeling uncertainty, allowing the generation of predictive distributions for unseen data points without requiring explicit model specification. Consequently, GPs have found applications in a variety of contexts.

The key to harnessing the power of GPs lies in the choice of kernel functions, also known as covariance functions. Rather than specifying a model, the GP framework revolves around selecting an appropriate kernel, transforming the problem into one of parameter estimation. Over time, researchers have developed various kernels, each tailored to specific scenarios, such as spatial data, time series data, and others (Genton, 2001). For instance, for spatiotemporal, a variety of kernels have been developed to capture unique characteristics and patterns (Gneiting, 2002; Stein, 2005).

The Radial Basis Function (RBF) kernel and Matérn kernels serve as prime examples of the diversity within the kernel family (Cressie and Wikle, 2015). The RBF kernel, renowned for its infinite differentiability, yields smooth functions, while Matérn kernels control the degree of smoothness by a kernel parameter, thereby accommodating both smooth and nonsmooth functions (Stein (1999)).

With each kernel bearing its own set of advantages and disadvantages, kernel selection, as a nontrivial task, often demands extensive domain knowledge.

Inspired by the potential of harnessing the strengths of multiple kernels concurrently, researchers have ventured into methods that involve kernel combinations, such as spectral mixtures (Wilson and Adams, 2013; Samo and Roberts, 2015; Remes et al., 2017), addition and/or multiplication of kernels (Duvenaud et al., 2011) such as mixture of RBF (Duvenaud et al., 2013), mixture of RBF, periodic (Per), linear (Lin), and rational quadratic (RQ) (Kronberger and Kommenda, 2013), mixture of RBF, RQ, Matérn and Per (Cheng et al., 2019; Verma and Engelhardt, 2020), mixture of RBF, Matérn $1/2$, $3/2$, $5/2$, as well as more sophisticated methods like Neural Kernel Networks (NKN, Sun et al. (2018) and Automatic Bayesian Covariance Discovery (ABCD, Lloyd et al. (2014). For instance, within the realm of spectral mixtures, Remes et al. (2017) proposed the Generalized Spectral Mixture (GSM) kernel, which is a product of three components all parametrized by GPs, representing frequencies, length-scales and mixture weights. In the category of summation and/or multiplication, Verma and Engelhardt (2020) utilized the sum of the RBF kernel and Matérn kernel with varying smoothness as the final kernel in their t-distribution Gaussian process latent variable model (tGPLVM), an extension to GPLVM (Lawrence, 2003; Lalchand et al., 2022), to characterize the latent features in single-cell RNA sequencing data.

In addition, methodological advances have facilitated the efficient discovery of optimal kernel mixtures. For example, NKN is reported to be more efficient than the Automatic Statistician, a gradient-based method. Simpson et al. (2021) utilized a transformer-based framework to generate mixture kernel recommendations. These studies underscore the advantages of employing mixed kernels in GP modeling, showcasing improved model fitting and more accurate predictions. By combining multiple kernels, the strengths of individual kernels can be leveraged to capture complex data patterns and relationships, potentially exceeding the capabilities of single kernels. Furthermore, the automatic selection of kernels optimizes model performance, reducing the reliance on extensive prior knowledge.

Another essential benefit of using mixture kernels in GP modeling lies in the improved interpretability. In contrast to complex, data-driven kernels, mixture kernels allow the decomposition of intricate patterns into simpler, distinct base kernels that are more readily interpretable. This technique, often termed decomposition, enables a more comprehensive understanding of the underlying data structure by simplifying complex patterns into their constitutive components. An illustrative example of this approach is the work of Duvenaud et al. (2013), who applied this decomposition technique for structure discovery in time series data. Their proposed mixture kernel comprised several base kernels, including RBF, periodic, linear, and rational quadratic kernels, enabling the dissection of time-series data patterns into components such as long-term trends, annual periodicity, and medium-term deviations. In a similar vein, the ABCD approach also employed decomposition, albeit with a different set of base kernels.

The identifiability of parameters within a single Matérn kernel has previously been explored, with the microergodic parameter uniquely identified as the only identifiable parameter, as outlined in Stein (1999). Tang et al. (2022) examined the identifiability of parameters within a single Matérn kernel with nuggets. Despite the prevalent use and interpretation of mixture kernels, their theoretical properties including identifiability and interpretability of parameters within kernel components, to the best of our knowledge, remain underexplored. A related critical question pertains to the common practice of using kernels with varying degrees of smoothness for enhanced flexibility. In this work, we turn our attention to the additive kernel in univariate GPs and multiplicative (separable) kernel in multivariate GPs, specifically focusing on the mixture of the widely-used Matérn kernel. We highlight the following novel findings:

- The smoothness of an additive mixture kernel is completely determined by the least smooth component.
- For additive mixture of Matérn kernels, the identifiability is confined only to a single parameter, also known as the microergodic parameter that is associated with the least smooth kernel component.
- For multivariate GPs with multiplicative separable kernels, the multiplicative matrix that controls the correlation structure among the response variables is identifiable up to a multiplicative constant.
- Our conclusions extend beyond the specific case of Matérn kernels, demonstrating applicability to a wider range of mixture kernels.

Our study aims to deepen the understanding of mixture kernel identifiability and interpretability, as well as to clarify the practical benefits of using kernels with varying degrees of smoothness. Our theoretical assertions are supported by both simulations and real-world applications. Details regarding the proofs of our theories and numerical experiments can be found in the Appendix.

2 Gaussian process, kernels and parameter inference

This section serves to define key terms and outline the parameter inference algorithm integral to the forthcoming theory and simulation sections.

A GP is a random function where any finite set of its realizations follows a multivariate normal distribution, characterized by a mean function μ and a covariance function K (Rasmussen and Williams, 2006).

Definition 1. f is said to follow a Gaussian process in domain Ω with a mean function $\mu : \Omega \rightarrow \mathbb{R}$ and a covariance function $K : \Omega \times \Omega \rightarrow \mathbb{R}$ if for any $x_1, \dots, x_n \in \Omega$,

$$[f(x_1), \dots, f(x_n)]^\top \sim N(v, \Sigma), \text{ where } v = [\mu(x_1), \dots, \mu(x_n)]^\top, \Sigma_{ij} = K(x_i, x_j).$$

For the purpose of this study, we assume $\mu = 0$, adhering to common practice and for the sake of simplicity. If the mean is not zero, a data transformation can be applied to achieve this. This approach is often adopted in machine learning and statistical analysis to simplify calculations and comply with certain algorithmic requirements (Rasmussen and Williams, 2006; Murphy, 2012).

As a consequence, the behavior of a GP is primarily determined by its kernel function. In this study, we assume the domain $\Omega = \mathbb{R}^p$ and our focus is on the selection of kernels that are widely recognized and commonly used in machine learning.

Definition 2. The RBF kernel, also known as the squared exponential kernel of Gaussian kernel is given by:

$$K(x, x') = \sigma^2 \exp(-\alpha \|x - x'\|^2).$$

The parameter σ^2 is called the spatial variance or partial sill that controls the point-wise variance, while α is called the (length) scale, range, or decay that controls the spatial dependency. A key characteristic of RBF is its smoothness, defined as follows:

Definition 3. A Gaussian process f is said to be mean-square continuous (MSC) if $\mathbb{E}(f(x+h) - f(x))^2 \xrightarrow{h \rightarrow 0} 0$ for any $x \in \mathbb{R}^p$. f is said to be mean-square differentiable (MSD) if $\lim_{h \rightarrow 0} \frac{f(x+h) - f(x)}{h}$ exists in the mean-square topology, and the limiting process is called the derivative process of f , denoted by f' . Similarly, the d -times mean-square differentiable (d -MSD) GPs can be defined inductively.

In particular, the above-defined RBF kernel is infinitely differentiable. However, oversmoothing can be problematic in prediction (Stein, 1999), leading to the popularity of the following flexible family of kernels that allow for varying smoothness:

Definition 4. The Matérn kernel is given by

$$K(x, x') = \frac{\sigma^2 2 \left(\frac{\alpha}{2} \|x - x'\|\right)^\nu}{\Gamma(\nu)} K_\nu(\alpha \|x - x'\|)$$

where K_ν is the modified Bessel function of the second kind. When $\nu = 1/2$, the Matérn kernel becomes the exponential kernel:

$$K(x, x') = \sigma^2 \exp(-\alpha \|x - x'\|)$$

The additional parameter ν is called the smoothness, since the smoothness of a Matérn GP is exactly $\lceil \nu \rceil - 1$. Inferring ν is known to be a particularly challenging problem, both from the theoretical and empirical perspectives (Zhang, 2004). In practice, ν is usually set to $1/2, 3/2, 5/2, \dots$ due to the simplified analytic form of the modified Bessel function.

The most straightforward estimator of the parameters σ^2 and α is the maximum likelihood estimator (MLE). In practice, optimizers such as Adam (Kingma and Ba, 2015) or stochastic gradient descent (SGD) are used to maximize the log-likelihood.

3 Univariate GP: additive kernels

In this section, we investigate the smoothness of mixture kernels and the identifiability of parameters in the additive mixture of Matérn kernels in the context of a univariate response variable. We note here that all the theorems presented are framed in an asymptotic context.

Consider K_1, \dots, K_L as L kernels with d_l -MSD. Define $K = \sum_{l=1}^L w_l K_l$ where $\sum_{l=1}^L w_l = 1$ and $w_l \geq 0$.

Theorem 1. K is $d := \min_l \{d_l\}$ -times MSD, but not $d + 1$ -times MSD, so the smoothness of K is determined by the least smooth component.

Beyond smoothness, we discuss the identifiability of the parameters in the mixture kernel, which relies on the notion of equivalence of measures.

Definition 5. Two measures \mathbb{P}_1 and \mathbb{P}_2 are said to be equivalent, i.e., $\mathbb{P}_1 \equiv \mathbb{P}_2$, if they are absolutely continuous with respect to each other; i.e., $\mathbb{P}_1(B) = 0 \iff \mathbb{P}_2(B) = 0$. Two GPs are equivalent if the corresponding Gaussian random measures are equivalent.

As a consequence, two equivalent GPs cannot be distinguished by any finite number of realizations (Stein, 1999). Specifically, given a family of GPs parametrized by θ , if $\mathbb{P}_{\theta_1} \iff \mathbb{P}_{\theta_2}$ with $\theta_1 \neq \theta_2$, then θ is not identifiable since we cannot distinguish between θ_1 and θ_2 . As a corollary, there does not exist any **consistent** estimator for θ .

Now we can study the identifiability of the mixture Matérn kernel $K = \sum_{l=1}^L w_l K_l$, where K_l is the Matérn kernel with parameters $(\sigma_l^2, \alpha_l, \nu_l)$, given known ν_l 's in ascending order $\nu_1 < \nu_2 < \dots < \nu_L$ with $\nu_l - \nu_{l-1} \geq 1$ for different smoothness.

Theorem 2. Let $K = \sum_l w_l K_l$ and $\tilde{K} = \sum_l \tilde{w}_l \tilde{K}_l$ be two kernels represented as linear combinations of Matérn kernels K_l 's and \tilde{K}_l with parameters $(\sigma_l^2, \alpha_l, \nu_l)$ and $(\tilde{\sigma}_l^2, \tilde{\alpha}_l, \nu_l)$.

(i) When $p = 1, 2, 3$, Then $K \equiv \tilde{K}$ if $w_1 \sigma_1^2 \alpha_1^{2\nu_1} = \tilde{w}_1 \tilde{\sigma}_1^2 \tilde{\alpha}_1^{2\nu_1}$.

(ii) When $p \geq 5$, Then $K \equiv \tilde{K}$ if

$$w_1 \sigma_1^2 \alpha_1^{2\nu_1} = \tilde{w}_1 \tilde{\sigma}_1^2 \tilde{\alpha}_1^{2\nu_1}, \quad w_2 \sigma_2^2 \alpha_2^{2\nu_2} - \nu_1 w_1 \sigma_1^2 \alpha_1^{2(\nu_1+1)} = \tilde{w}_2 \tilde{\sigma}_2^2 \tilde{\alpha}_2^{2\nu_2} - \nu_1 \tilde{w}_1 \tilde{\sigma}_1^2 \tilde{\alpha}_1^{2(\nu_1+1)}.$$

Consequently, no single parameter is identifiable. The only identifiable parameter when $p \leq 3$ is $w_1 \sigma_1^2 \alpha_1^{2\nu_1}$, known as the microergodic parameter (Stein, 1999).

Interestingly, the case of $p = 4$ is missing here. We hypothesize that it aligns with the case of $p \geq 5$. However, providing a proof remains challenging. It is also worth noting that the issue of identifiability persists even for a single Matérn kernel, as highlighted in the existing literature (Zhang, 2004; Anderes, 2010; Li et al., 2023).

Corollary 1. The mixture kernel K is equivalent to K_1 , that is, the mixture kernel is equivalent to its least smooth component. Furthermore, the mean squared error (MSE) of the mixture kernel K is asymptotically equal to the MSE of K_1 .

Theorem 2 implies that interpreting w_l as the weight of each component is often misleading due to its nonidentifiability. Furthermore, Corollary 1 suggests the use of a single Matérn kernel in lieu of the linear mixture kernel. Both assertions are supported by the simulation study in Section 5 and the real-world application in Section 6.

An alternative strategy is to assume the same smoothness across mixing components, i.e., $\nu_1 = \nu_2, \dots, \nu_L$. In this case, we prove that no single parameter is identifiable. The complete theorem, proof, and simulation are in the Appendix.

When considering real-world data, it is often the case that the observed outcomes are noisy, which is frequently modeled as an i.i.d. Gaussian with variance denoted by τ^2 , commonly referred as the "nugget". The inclusion of such a noise term is essential to capture the inherent variability in the data. Equivalently, the model can be formulated as noiseless by adjusting the kernel to be $K(x, x') + \tau^2 \mathbf{1}_{\{x=x'\}}$. The following corollary shows that the noise, or nugget, does not impact the identifiability and interpretability of the mixture of Matérn kernels as shown in Theorem 2.

Corollary 2. Let τ^2 and $\tilde{\tau}^2$ be the noise variance of K and \tilde{K} . If $\tau^2 \neq \tilde{\tau}^2$, then $K \not\equiv \tilde{K}$. If $\tau^2 = \tilde{\tau}^2$, the previous results in Theorem 2 hold.

In essence, while the presence of noise or "nugget" captures real-world data variability, it does not obscure or alter the fundamental characteristics of the mixture of Matérn kernels as established in our theorems.

4 Multivariate GP: multiplicative kernels

In this section, we shift our focus to multivariate GPs, also known as multi-output or multi-task GPs, which are applicable to datasets with multiple response variables.

Definition 6. $f : \Omega \rightarrow \mathbb{R}^m$ is said to follow a m -variate GP in domain Ω with zero mean and cross-covariance function $K : \Omega \times \Omega \rightarrow \text{PD}(m)$, where $\text{PD}(m)$ is the space of all m by m positive definite matrices, if for any x_1, \dots, x_n :

$$[f(x_1), \dots, f(x_n)]^\top \sim MN(0, \Sigma),$$

where MN represents matrix Gaussian distribution and Σ consists of $m \times m$ blocks $\Sigma_{ij} = K(x_i, x_j)$.

The construction of valid cross-covariance kernels is a pivotal yet challenging aspect of multivariate GPs (Gneiting, 2002; Apanasovich and Genton, 2010; Genton and Kleiber, 2015). A popular kernel that is widely used due to its simplicity and seemingly interpretability is the multiplicative kernel, also known as a separable kernel. This kernel admits the form $K(x, y) = AK_0(x, y)$ where K_0 is a standard kernel for univariate GP like Matérn while $A \in \text{PD}(m)$ is a positive definite matrix reflecting the correlation between response variables. The following theorem investigates the identifiability of the multiplicative cross-covariance kernel.

Theorem 3. (i) When K_0 is Matérn with parameters (σ^2, α, ν) where ν is given, then $K \equiv \tilde{K}$ if $\sigma^2 \alpha^{2\nu} A = \tilde{\sigma}^2 \tilde{\alpha}^{2\nu} \tilde{A}$. That is, the identifiable parameter is $\sigma^2 \alpha^{2\nu} A$. Hence A is identifiable up to a multiplicative constant and the correlation structure is identifiable.

(ii) Let K_0 be an arbitrary kernel with spectral density ρ_0 satisfying:

$$\exists \gamma \in \mathcal{W}_{[-b, b]^m}, 0 < b < \infty, c_1, c_2 > 0, \text{ s.t.}, c_1 \gamma(\omega)^2 \leq \rho_0(\omega) \leq c_2 \gamma(\omega)^2,$$

where $\mathcal{W}_{[-b, b]^d}$ is the space of Fourier transforms of $L^2(\mathbb{R}^p)$ functions with compact support $[-b, b]^d$ (see the Appendix for more details). If θ is a microergodic parameter of K_0 , such that $\int_{\mathbb{R}^p} \frac{1}{\gamma^4(\omega)} \left(\frac{\rho(\omega)}{\theta} - \frac{\tilde{\rho}(\omega)}{\tilde{\theta}} \right)^2 d\omega < 0$ if $\theta = \tilde{\theta}$, then $K \equiv \tilde{K}$ if $\sigma^2 \alpha^{2\nu} A = \tilde{\sigma}^2 \tilde{\alpha}^{2\nu} \tilde{A}$. That is, the identifiable parameter is θA , hence A is identifiable up to a multiplicative constant and the correlation structure is identifiable.

Note that (i) is a special case of (ii), as the Matérn kernel satisfies the additional assumptions in (ii). This theorem positively supports the utilization of the multiplicative kernel and the interpretation that A_{ij} measures the correlation between the i -th response variable and the j -th response variable.

5 Simulation

In this section, we will validate the proposed theories by conducting three simulation studies. The first simulation demonstrates Theorem 1 using a mixture of Matérn kernels, highlighting that the smoothness of the sample path (e.g., a realization of the GP) is determined by the least smooth component. The second simulation supports Theorem 2 using a mixture kernel of Matérn kernels with varying smoothness. It shows that none of the single parameters are identifiable, and only the proposed microergodic parameter can be identified. Finally, the third simulation showcases Theorem 3, suggesting that the multiplicative matrix is identifiable up to a multiplicative constant.

5.1 Simulation 1 - Univariate GP: Smoothness

In the first simulation, we show that the smoothness of the sample path is determined by the smoothness of the least smooth kernel. We generate 200 samples as an equidistant sequence ranging

from 0 – 10. We consider the following mixture kernel: $K = \sum_{l=1}^3 w_l K_l$, where K_l is the Matérn kernel with smoothness parameter ν_l being $\frac{2l-1}{2}$ and $\sum_{l=1}^L w_l = 1$, $w_l \geq 0$. We randomly sample Y from multivariate normal distribution with kernel function as the mixture kernel, Matérn with $\nu = 1/2, 3/2, 5/2$. The resulting sample paths are summarized in Figure 1.

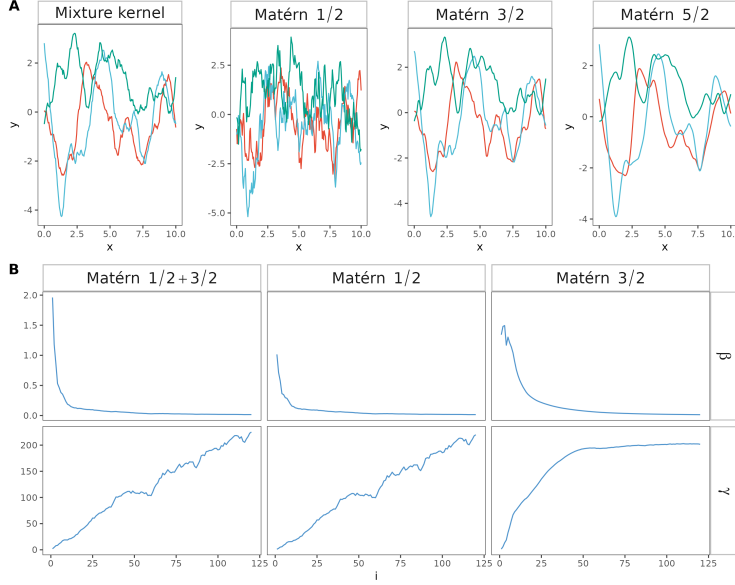


Figure 1: Smoothness of Matérn kernels. Sample path of (A) Mixture kernel (B) Matérn 1/2 (C) Matérn 3/2 (D) Matérn 5/2. (E) Numerical examination of Theorem 1.

Our results clearly indicate that the Matérn kernel with $\nu = 1/2$ exhibits the least degree of smoothness (continuous but not differentiable), and the smoothness increases with ν . The smoothness of the mixture kernel is predominantly influenced by the Matérn kernel with $\nu = 1/2$. When comparing the sample path of the mixture kernel to those of the Matérn kernels with $\nu = 3/2$ and $\nu = 5/2$, it is evident that the mixture kernel demonstrates a degree of smoothness similar to the Matérn kernels with $\nu = 1/2$.

To better demonstrate the smoothness of the mixture kernel and its least component, we further examine the continuity and MSD of the mixture kernel and its mixing components empirically. For a fixed $x_0 = 0$, let $x_i = 1/i$ for $i = 1, 2, \dots$, and we generate y_i^l from the GP, where $l = 1, \dots, T$ denotes the index of replicates. This allows us to approximate $\lim_{x \rightarrow 0} \mathbb{E}(f(x) - f(0))^2$ by $\beta_i = \frac{1}{T} \sum_{l=1}^T (y_i^l - y_0^l)^2$. As per Definition 3, the GP is continuous if and only if $\beta_i \rightarrow 0$. Similarly, we can approximate $\lim_{x \rightarrow 0} \mathbb{E} \left(\frac{f(x) - f(0)}{x} \right)^2$ by $\gamma_i = \frac{1}{T} \sum_{l=1}^T \left(\frac{y_i^l - y_0^l}{x_i} \right)^2$. The GP is mean-square differentiable if and only if $\lim_{i \rightarrow \infty} \gamma_i$ exists. Specifically, for the mixture of Matérn 1/2 and 3/2 and Matérn 1/2, while $\beta_i \rightarrow 0$, γ_i does not converge (Figure 1 first two columns), which indicates that both the mixture kernel and Matérn 1/2 are continuous but not differentiable. However, for Matérn 3/2 (Figure 1 third column), $\beta_i \rightarrow 0$ and γ_i converges, implying that Matérn 3/2 is continuous and differentiable.

These empirical observations strongly support the claims made in Theorem 1, which suggests that the inclusion of smoother kernel components in the mixture does not inherently enhance the overall smoothness of the mixture kernel.

5.2 Simulation 2 - Univariate GP: Components with different smoothness

In the second simulation, our aim is to assess parameter identifiability in a GP with a mixture kernel consisting of Matérn kernels with distinct smoothness. The mixture kernel is denoted as $K = \sum_{l=1}^3 w_l K_l$, where K_l is a Matérn kernel with parameters $(\sigma_l^2, \alpha_l, \nu_l)$. For this simulation, we set $\nu_1 = 1/2, \nu_2 = 3/2, \nu_3 = 5/2$. Theorem 2 indicates that the only identifiable parameter is

$w_l \sigma_l^2 \alpha_l$, while all other parameters remain unidentifiable. In this scenario, the identifiable parameter, also known as the microergodic parameter, is associated with the least smooth component, i.e., the Matérn 1/2 kernel. We will assess parameter inference by comparing estimated values to their true values across different training sample sizes. For this experiment, we generate n samples, ranging from 20, 50, 100, 500. For each sample size, we replicate the simulation 100 times.

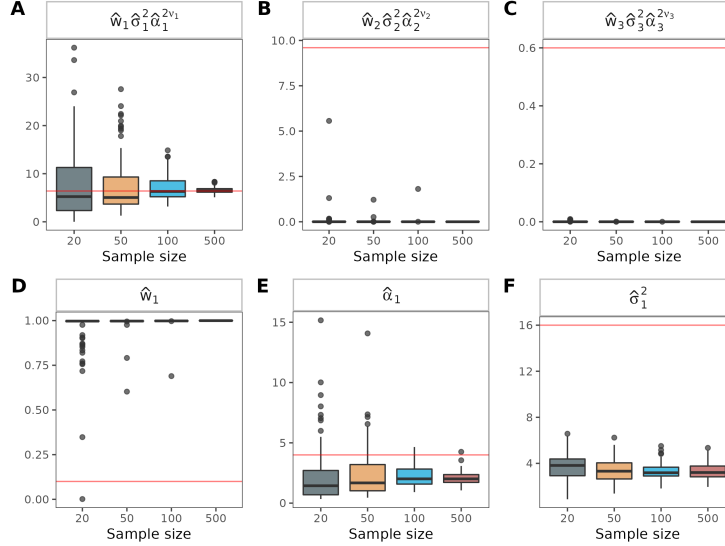


Figure 2: Parameter estimation. (A) Only the microergodic parameter $w_1 \sigma_1^2 \alpha_1$ is identifiable. (B-F) other parameters are not identifiable. The red line indicates the true value.

The results provide persuasive support for Theorem 2 that, in the context of additive mixture of Matérn kernels with distinct smoothness, only the MLE of the microergodic parameter $w_1 \sigma_1^2 \alpha_1$ for the least smooth component converges to the true value. The MLEs for all other parameters do not converge to their respective true values, highlighting the unique identifiability of the parameters in the least smooth component within the additive mixture kernel framework. Such results are robust in terms of optimizer choice and consistent as the sample size increases to 3000 (details in the Appendix).

5.3 Simulation 3 - Multivariate GP

Next, we turn our attention to multivariate GPs with a separable kernel. We define the separable kernel as $K = AK_0$. Here, we select Matérn 1/2 as K_0 , characterized by the parameters (σ^2, α) . Our Theorem 3 suggests that only $A\alpha^{2\nu}\sigma^2$ is identifiable. To verify this, we adopt a bivariate setup where A is a 2×2 positive definite matrix. In this simulation, the sample size n varies from 50, 100, 200, 400. For each sample size, we replicate the simulation 100 times.

The parameter estimates are summarized in Figure 3. Evidently, only the MLE of the microergodic parameter $A\sigma^2\alpha^{2\nu}$ converges to its true value. These findings reinforce the identifiability and interpretability of the separable kernel. This understanding is critical for the interpretation and application of separable kernels in real-world situations.

6 Application

Motivated by the findings in our theoretical and simulation studies, we proceed to compare the performance of the mixture kernel with varying smoothness and the least smooth component within that mixture only, in real-world data applications. In this section, we will revisit several applications in previous studies (Rasmussen and Williams (2006), Wilson et al. (2014), Sun et al. (2018)), illustrating that the mixture kernel achieves prediction performance comparable to the least smooth kernel component within the mixture.

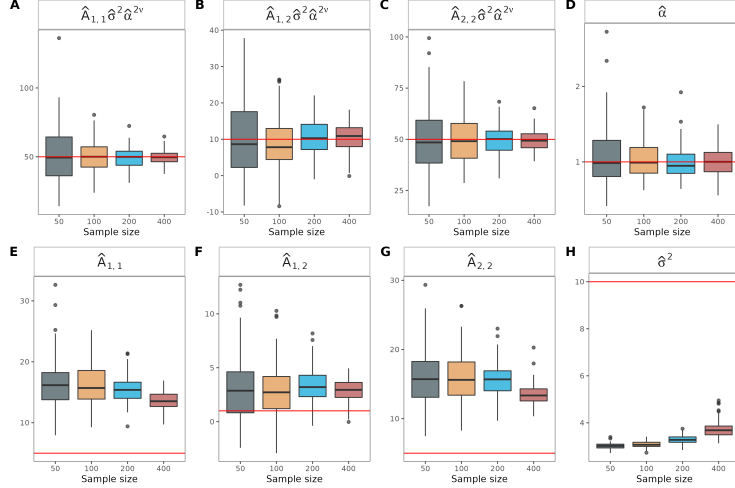


Figure 3: Parameter estimation. (A-C) Only the microergodic parameter $A\sigma^2\alpha^{2\nu}$ is identifiable (D-E) All other parameters are not identifiable. The red dotted line indicates the true value.

6.1 Application 1 - Image prediction

For our first real-data application, we delve into the domain of image analysis. GP has been widely used to predict missing image (Wilson et al. (2014), Sun et al. (2018)). This task of image prediction is an exemplary context for assessing kernel performance in discerning local correlation patterns, providing a visually intuitive framework for comparative analysis.

We employ a handwritten zero image from the MNIST dataset (LeCun et al. (1998)) for this analysis; we extract a 20×20 section from the center of the original 100×100 image to serve as our test image. This results in a training dataset of 9600 pixels and a testing dataset with 400 pixels (Figure 4A). The input for this analysis comprises the 2-D pixel locations, with the corresponding pixel intensities serving as the response. To reconstruct the missing area, we train GP regression models with both the mixture kernel with varying smoothness and a single Matérn 1/2 kernel on the training dataset, and subsequently make predictions on the testing dataset. Specifically, we employ a mixture of three Matérn kernels of smoothness 1/2, 3/2, 5/2. Our analysis seeks to demonstrate the similarities in performance between the mixture kernel and the least smooth component within that mixture, i.e., Matérn 1/2, in terms of prediction in the missing image area.

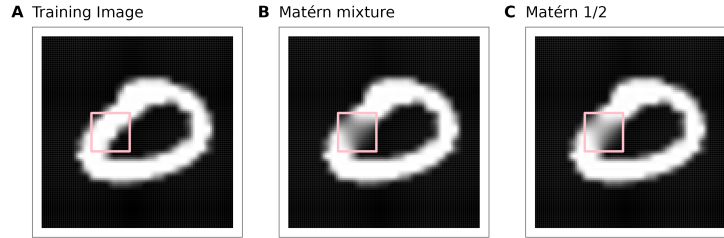


Figure 4: Texture exploration in diamond plate. (A) Training image. (B) Prediction of the mixture kernel. The area in the pink box represents the testing image area. (C) Prediction of the Matérn 1/2 kernel.

The predictions generated by both the mixture kernel and the Matérn 1/2 kernel demonstrate a remarkable similarity, as shown in Figure 4. This observation suggests that the mixture kernel and a single Matérn 1/2 kernel have comparable performance. The close alignment between their predictions implies that using the mixture kernel does not yield significant advantages over the least smooth kernel component in this specific application, further reinforcing our theoretical findings (Theorem 2) regarding the dominance of the least smooth component in the mixture kernel.

6.2 Application 2 - Manua Loa CO₂

In this section, we extend our comparative analysis to the widely recognized Moana Loa CO₂ dataset from the Global Monitoring Laboratory's Repository as our benchmark for regression analysis (Tans and Keeling (2023)). Rasmussen and Williams (2006) employed this dataset to demonstrate that constructing a complex covariance function by combining several different types of simple covariance functions could yield an excellent fit to complex data. Consequently, we consider it to be a suitable choice for testing our theorem.

Specifically, we used the decimal date from 1960 to 2020 as our input and the monthly average CO₂ as our response. In this context, we compare the performance of Matérn mixture $1/2 + 3/2$, $1/2 + 3/2 + 5/2$, $3/2 + 5/2$ and three single Matérn kernels ($1/2$, $3/2$, $5/2$). The dataset consists of 720 records. We undertook an extensive assessment, varying the training sample size from 5% to 95% and keeping the test sample size as the remaining data. For each training sample size, we conducted 10 simulations using different random splits of the dataset as replications. This strategy allows for a robust and thorough evaluation of the prediction accuracy of both the mixture kernel and the single kernel component in the context of a regression problem with varying training sample sizes. We use the MSE to quantify the prediction accuracy (Figure 5).

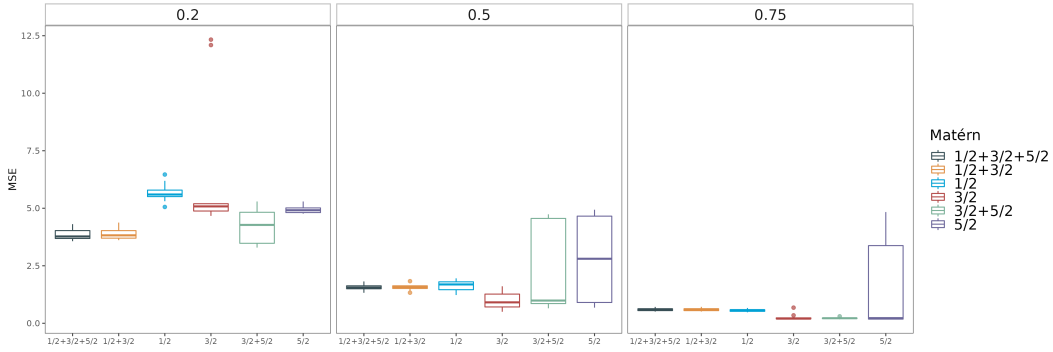


Figure 5: Manua Loa CO₂ prediction MSE in test dataset with 20%, 50% and 75% training dataset. Boxplot are colored by different Matérn kernels.

The Matérn mixture kernel $1/2 + 3/2 + 5/2$ aligned closely with $1/2 + 3/2$ across all experiments. Furthermore, these three Matérn mixture kernels ($1/2 + 3/2 + 5/2$, $1/2 + 3/2$, $1/2$) converge when the training sample size ratio reaches 50%. This empirical finding supports the theoretical equivalence of these three GPs as posited in Theorem 2. Similarly, the Matérn mixture $3/2 + 5/2$ kernel and the standalone Matérn $3/2$ kernel converge from a 65% sample size, lending empirical weight to their theoretical equivalence and their equivalence in MSE as stated in Corollary 1.

Matérn $3/2$ kernel has exceptional performance across all experiments. However, its influential performance is diluted when coupled with the less smooth component, Matérn $1/2$. On the contrary, when mixed with the smoother Matérn $5/2$ component, the worse performance of the latter is overshadowed by Matérn $3/2$. These behaviors lend empirical weight to our Theorem 2, suggesting that in the asymptotic sense, the mixture kernel is dominated by its least smooth component.

A noteworthy trend is the inequivalence of the Matérn mixture kernel and its least component with a limited training sample (training sample size $< 50\%$). We consider such scenario as the "finite" sample scenario in contrast to our focus on the infinite sample scenario, i.e. asymptotic theory. Theoretically, while the Matérn mixture kernels $1/2 + 3/2 + 5/2$, $1/2 + 3/2$, and the standalone Matérn $1/2$ kernel are deemed equivalent, and the Matérn mixture kernel $3/2 + 5/2$ is akin to the Matérn $3/2$ kernel, their practical agreement points, i.e. 50% and 65%, differed with limited training samples. Although securing a conclusive theoretical support for the finite sample regime is challenging, we managed to provide some insights to interpret our findings. To do so, we have to delve further into the proof of Stein (1993)'s Theorem 1, which guides us to Theorem 3.1 in Stein (1990). The proof suggests that the relative difference between the MSEs rests on the tail of the series. This difference is influenced by both the sample size (denoted as N in Stein (1990)) and by b_{jk} and μ_j , as defined on the same page. For a fixed sample size, smaller values of $(b_{jk} + \mu_j \mu_k)^2$ result in a

smaller relative difference between MSEs. By the definition of b_{jk} and μ_j , the more "different" the two kernels are, in other words, the more "significant" the additional smoother components become — the greater the difference between the MSEs will be.

7 Discussion and future work

In this study, we delved into the identifiability and interpretability of parameters in GPs with various mixture kernels in the asymptotic scenario and fixed domain, including the additive kernel and separable kernels. We formulated a series of theorems clarifying the identifiable parameters in these kernel structures, and further corroborated our theorems through multiple simulations and real-data applications. Our simulation results convincingly demonstrated that in GPs with mixture kernels, the only identifiable parameter, known as the microergodic parameter, is associated with the least smooth kernel component. This discovery has profound implications for parameter interpretation in the context of GPs with mixture kernels. Empirical evidence from image data analysis and Manua Loa CO₂ regression studies further reinforce these discoveries. Despite the inclusion of kernels with varying smoothness in the mixture kernel, the performance of the mixture kernel closely paralleled that of the least smooth kernel component within it when the sample size is large enough, regardless of its performance. This observation suggests that the inclusion of kernels with different smoothness does not necessarily improve the prediction accuracy. In fact, due to various real world factors including limited training samples, optimization and more, determining a clear winner in performance between Matérn mixture kernel and single Matérn kernel proves to be a challenging task. Lastly, in the case of multivariate GPs with separable kernels, our theoretical and simulation results show that the correlation structure is identifiable up to a multiplicative constant. This result underlines that the interpretability of separable kernels mainly resides in the relative correlation structure, rather than individual parameters.

Although our study has provided substantial insight on the identifiability and interpretability of parameters in GPs with various mixture kernel types, it also opens several exciting avenues for future research. First, our analysis primarily focuses on Matérn kernels, and it would be intriguing to extend this framework to other families of kernels, such as the periodic kernel. Such an extension would provide a more comprehensive understanding of parameter identifiability and predictive performance across a broader spectrum of kernel types. Second, our work has so far considered the cases where $p \leq 3$ or $p \geq 5$. However, extending this to $p = 4$ presents a substantial challenge due to the lack of mathematical tools to determine whether two Gaussian random measures are equivalent or not. Third, our observations in the Mauna Loa CO₂ example underscore the need for further exploration in the finite sample scenario. Potential avenues for future research include investigating the convergence rates of both the Matérn mixture kernel and the single Matérn kernel. Lastly, while we have identified the microergodic parameters that are theoretically identifiable in mixture kernels, an important direction for future work involves finding consistent estimators for these kernel parameters. This would entail developing novel estimation techniques or adapting existing ones to reliably estimate the parameters in practice, thereby enhancing the practical utility of our theoretical findings. These endeavors will not only extend the theoretical foundations of GPs with mixture kernels, but will also broaden their applicability across various real-world scenarios.

Acknowledgments and Disclosure of Funding

We express our sincere gratitude to anonymous reviewers and the Area Chair for their insightful comments and constructive feedback, which significantly enhanced the quality and clarity of this work. DL was supported by the NIH/NCATS award UL1 TR002489, NIH/NHLBI award R01 HL149683 and NIH/NIEHS award P30 ES010126. YL was partially supported by NIH awards R01AG079291 and U01HG011720. All the codes for replicating the analysis and parameter estimates are available at: https://github.com/JiawenChenn/GP_mixture_kernel.

References

- Anderes, E. (2010). On the consistent separation of scale and variance for Gaussian random fields. *The Annals of Statistics*.
- Apanasovich, T. V. and M. G. Genton (2010). Cross-covariance functions for multivariate random fields based on latent dimensions. *Biometrika* 97(1), 15–30.
- Bachoc, F., E. Porcu, M. Bevilacqua, R. Furrer, and T. Faouzi (2022). Asymptotically equivalent prediction in multivariate geostatistics. *Bernoulli* 28(4), 2518–2545.
- Banerjee, S., B. P. Carlin, and A. E. Gelfand (2014). *Hierarchical modeling and analysis for spatial data*. CRC press.
- Cheng, L., S. Ramchandran, T. Vatanen, N. Lietzén, R. Lahesmaa, A. Vehtari, and H. Lähdesmäki (2019). An additive Gaussian process regression model for interpretable non-parametric analysis of longitudinal data. *Nature Communications* 10(1), 1798.
- Cressie, N. and C. K. Wikle (2015). *Statistics for spatio-temporal data*. John Wiley & Sons.
- Duvenaud, D., J. Lloyd, R. Grosse, J. Tenenbaum, and G. Zoubin (2013, 17–19 Jun). Structure discovery in nonparametric regression through compositional kernel search. In S. Dasgupta and D. McAllester (Eds.), *Proceedings of the 30th International Conference on Machine Learning*, Volume 28 of *Proceedings of Machine Learning Research*, Atlanta, Georgia, USA, pp. 1166–1174. PMLR.
- Duvenaud, D. K., H. Nickisch, and C. Rasmussen (2011). Additive Gaussian processes. In J. Shawe-Taylor, R. Zemel, P. Bartlett, F. Pereira, and K. Weinberger (Eds.), *Advances in Neural Information Processing Systems*, Volume 24. Curran Associates, Inc.
- Genton, M. G. (2001). Classes of kernels for machine learning: a statistics perspective. *Journal of machine learning research* 2(Dec), 299–312.
- Genton, M. G. and W. Kleiber (2015). Cross-Covariance Functions for Multivariate Geostatistics. *Statistical Science* 30(2), 147 – 163.
- Gneiting, T. (2002). Nonseparable, stationary covariance functions for space–time data. *Journal of the American Statistical Association* 97(458), 590–600.
- Kingma, D. P. and J. Ba (2015). Adam: A method for stochastic optimization. In Y. Bengio and Y. LeCun (Eds.), *3rd International Conference on Learning Representations, ICLR 2015, San Diego, CA, USA, May 7-9, 2015, Conference Track Proceedings*.
- Kronberger, G. and M. Kommenda (2013). Evolution of covariance functions for Gaussian process regression using genetic programming.
- Lalchand, V., A. Ravuri, and N. D. Lawrence (2022). Generalised gplvm with stochastic variational inference. In *International Conference on Artificial Intelligence and Statistics*, pp. 7841–7864. PMLR.
- Lawrence, N. (2003). Gaussian process latent variable models for visualisation of high dimensional data. In S. Thrun, L. Saul, and B. Schölkopf (Eds.), *Advances in Neural Information Processing Systems*, Volume 16. MIT Press.
- LeCun, Y., C. Cortes, and C. J. Burges (1998). The mnist database of handwritten digits. <http://yann.lecun.com/exdb/mnist/>. Accessed: 2023-08-01.
- Li, D., W. Tang, and S. Banerjee (2023). Inference for gaussian processes with matérn covariogram on compact riemannian manifolds. *Journal of Machine Learning Research* 24(101), 1–26.
- Lloyd, J. R., D. Duvenaud, R. Grosse, J. B. Tenenbaum, and Z. Ghahramani (2014). Automatic construction and natural-language description of nonparametric regression models.
- Murphy, K. P. (2012). *Machine learning: a probabilistic perspective*. MIT press.

- Pedregosa, F., G. Varoquaux, A. Gramfort, V. Michel, B. Thirion, O. Grisel, M. Blondel, P. Prettenhofer, R. Weiss, V. Dubourg, J. Vanderplas, A. Passos, D. Cournapeau, M. Brucher, M. Perrot, and E. Duchesnay (2011). Scikit-learn: Machine learning in Python. *Journal of Machine Learning Research* 12, 2825–2830.
- Rasmussen, C. E. and C. K. I. Williams (2006). *Gaussian processes for machine learning*. Adaptive computation and machine learning. MIT Press.
- Remes, S., M. Heinonen, and S. Kaski (2017). Non-stationary spectral kernels. In I. Guyon, U. V. Luxburg, S. Bengio, H. Wallach, R. Fergus, S. Vishwanathan, and R. Garnett (Eds.), *Advances in Neural Information Processing Systems*, Volume 30. Curran Associates, Inc.
- Samo, Y.-L. K. and S. Roberts (2015). Generalized spectral kernels.
- Simpson, F., I. Davies, V. Lalchand, A. Vullo, N. Durrande, and C. E. Rasmussen (2021). Kernel identification through transformers. In M. Ranzato, A. Beygelzimer, Y. Dauphin, P. Liang, and J. W. Vaughan (Eds.), *Advances in Neural Information Processing Systems*, Volume 34, pp. 10483–10495. Curran Associates, Inc.
- Stein, M. (1990). Uniform asymptotic optimality of linear predictions of a random field using an incorrect second-order structure. *The Annals of Statistics* 18(2), 850–872.
- Stein, M. L. (1993). A simple condition for asymptotic optimality of linear predictions of random fields. *Statistics & Probability Letters* 17(5), 399–404.
- Stein, M. L. (1999). *Interpolation of spatial data: some theory for kriging*. Springer Science & Business Media.
- Stein, M. L. (2005). Space–time covariance functions. *Journal of the American Statistical Association* 100(469), 310–321.
- Sun, S., G. Zhang, C. Wang, W. Zeng, J. Li, and R. Grosse (2018, 10–15 Jul). Differentiable compositional kernel learning for Gaussian processes. In J. Dy and A. Krause (Eds.), *Proceedings of the 35th International Conference on Machine Learning*, Volume 80 of *Proceedings of Machine Learning Research*, pp. 4828–4837. PMLR.
- Tang, W., L. Zhang, and S. Banerjee (2022). On identifiability and consistency of the nugget in gaussian spatial process models. *Journal of the Royal Statistical Society Series B: Statistical Methodology* 83(5), 1044–1070.
- Tans, P. and R. Keeling (2023). Trends in atmospheric carbon dioxide. <https://gml.noaa.gov/ccgg/trends/data.html>. Accessed: 2023-08-01.
- Verma, A. and B. E. Engelhardt (2020). A robust nonlinear low-dimensional manifold for single cell RNA-seq data. *BMC Bioinformatics* 21(1), 324.
- Wilson, A. and R. Adams (2013, 17–19 Jun). Gaussian process kernels for pattern discovery and extrapolation. In S. Dasgupta and D. McAllester (Eds.), *Proceedings of the 30th International Conference on Machine Learning*, Volume 28 of *Proceedings of Machine Learning Research*, Atlanta, Georgia, USA, pp. 1067–1075. PMLR.
- Wilson, A. G., E. Gilboa, A. Nehorai, and J. P. Cunningham (2014). Fast kernel learning for multidimensional pattern extrapolation. In Z. Ghahramani, M. Welling, C. Cortes, N. Lawrence, and K. Weinberger (Eds.), *Advances in Neural Information Processing Systems*, Volume 27. Curran Associates, Inc.
- Yadrenko, M. I. and A. V. Balakrishnan (1983). Spectral theory of random fields.
- Zhang, H. (2004). Inconsistent estimation and asymptotically equal interpolations in model-based geostatistics. *Journal of the American Statistical Association* 99(465), 250–261.

A Proof of Theorem 1

We first state a Lemma for determining the smoothness for a stationary GP.

Lemma 1 (Stein (1999)). *Let ρ be the spectral density of a GP with kernel K , then K is d -times mean squared differentiable if and only if*

$$\int \|\omega\|^{2d} \rho(\omega) d\omega < \infty.$$

Proof of Theorem 1. Let ρ_l be the spectral density of K_l , then the spectral density of K is given by $\rho = \sum_{l=1}^L \rho_l$ by the linearity of Fourier transform. Then by the smoothness of K_l and Lemma 1, we have $\int \|\omega\|^{2d} \rho_l(\omega) d\omega < \infty$. As a result,

$$\begin{aligned} \int \|\omega\|^{2d} \rho(\omega) d\omega &= \sum_{l=1}^L \int \|\omega\|^{2d} \rho_l(\omega) d\omega = \sum_{l=1}^L \int_{\|\omega\| \leq 1} \|\omega\|^{2d} \rho_l(\omega) d\omega + \sum_{l=1}^L \int_{\|\omega\| \geq 1} \|\omega\|^{2d} \rho_l(\omega) d\omega \\ &\leq \sum_{l=1}^L \int_{\|\omega\| \leq 1} \rho_l(\omega) d\omega + \sum_{l=1}^L \int \|\omega\|^{2d} \rho_l(\omega) d\omega < \infty, \end{aligned}$$

that is, K is d -times MSD. Similarly, K is not $d+1$ -times MSD since

$$\int \|\omega\|^{2(d+1)} \rho(\omega) d\omega = \sum_{l=1}^L \int \|\omega\|^{2(d+1)} \rho_l(\omega) d\omega \geq \int \|\omega\|^{2(d+1)} \rho_1(\omega) d\omega = \infty.$$

□

B Proof of Theorem 2

We first state a Lemma, also known as the integral test to determine whether two GPs are equivalent or not.

Lemma 2 (Yadrenko and Balakrishnan (1983), Zhang (2004)). *Let K_1 and K_2 be the kernels of two GPs P_1 and P_2 with spectral densities ρ_1 and ρ_2 . Then $P_1 \equiv P_2$ if*

1. *There exists $r > 0$ such that $\|\omega\|^r \rho_1(\omega)$ is bounded away from both zero and infinity as $\omega \rightarrow \infty$.*
2. *There exists $\delta > 0$ such that $\int_{\|\omega\| > \delta} \left(\frac{\rho_2(\omega) - \rho_1(\omega)}{\rho_1(\omega)} \right)^2 d\omega < \infty$.*

Proof of Theorem 2. Recall that the spectral densities of K_l are

$$\rho_l(\omega) = \frac{\sigma_l^2 \alpha_l^{2\nu_l}}{(\alpha_l^2 + \|\omega\|^2)^{\nu_l + \frac{p}{2}}}, \quad \rho(\omega) = \sum_{l=1}^L w_l \frac{\sigma_l^2 \alpha_l^{2\nu_l}}{(\alpha_l^2 + \|\omega\|^2)^{\nu_l + \frac{p}{2}}}, \quad \tilde{\rho}(\omega) = \sum_{l=1}^L \tilde{w}_l \frac{\tilde{\sigma}_l^2 \tilde{\alpha}_l^{2\nu_l}}{(\tilde{\alpha}_l^2 + \|\omega\|^2)^{\nu_l + \frac{p}{2}}}.$$

To apply the integral test, first, let $r = 2(\nu_1 + \frac{p}{2})$, then

$$\rho(\omega) \|\omega\|^r = \sum_{l=1}^L w_l \frac{\sigma_l^2 \alpha_l^{2\nu_l} \|\omega\|^r}{(\alpha_l^2 + \|\omega\|^2)^{\nu_l + \frac{p}{2}}} \xrightarrow{\omega \rightarrow \infty} w_1 \sigma_1^2 \alpha_1^{2\nu_1},$$

that is, bounded away from both 0 and ∞ as $\omega \rightarrow \infty$. Then we check the relative difference between the spectral densities ρ and $\tilde{\rho}$. Observe that when,

$$\rho(\omega) = \sum_{l=1}^L w_l \frac{\sigma_l^2 \alpha_l^{2\nu_l}}{(\alpha_l^2 + \|\omega\|^2)^{\nu_l + \frac{p}{2}}} = \frac{\sum_{l=1}^L w_l \sigma_l^2 \alpha_l^{2\nu_l} \prod_{j \neq l} (\alpha_j^2 + \|\omega\|^2)^{\nu_j + \frac{p}{2}}}{\prod_{l=1}^L (\alpha_l^2 + \|\omega\|^2)^{\nu_l + \frac{p}{2}}} =: \frac{\sum_{l=1}^L w_l \sigma_l^2 \alpha_l^{2\nu_l} p_l(\omega)}{\prod_{l=1}^L (\alpha_l^2 + \|\omega\|^2)^{\nu_l + \frac{p}{2}}},$$

where $p_l := \prod_{j \neq l} (\alpha_j^2 + \|\omega\|^2)^{\nu_j + \frac{p}{2}}$. Similarly,

$$\tilde{\rho}(\omega) = \frac{\sum_{l=1}^L \tilde{w}_l \tilde{\sigma}_l^2 \tilde{\alpha}_l^{2\nu_l} \tilde{p}_l(\omega)}{\prod_{l=1}^L (\tilde{\alpha}_l^2 + \|\omega\|^2)^{\nu_l + \frac{p}{2}}},$$

where $\tilde{p}_l := \prod_{j \neq l} (\tilde{\alpha}_j^2 + \|\omega\|^2)^{\nu_j + \frac{p}{2}}$. Observe that when $\|\omega\| \rightarrow \infty$,

$$\frac{\prod_{l=1}^L (\tilde{\alpha}_l^2 + \|\omega\|^2)^{\nu_l + \frac{p}{2}}}{\prod_{l=1}^L (\alpha_l^2 + \|\omega\|^2)^{\nu_l + \frac{p}{2}}} = \frac{\prod_{l=1}^L \left(1 + \frac{\tilde{\alpha}_l^2}{\|\omega\|^2}\right)^{\nu_l + \frac{p}{2}}}{\prod_{l=1}^L \left(1 + \frac{\alpha_l^2}{\|\omega\|^2}\right)^{\nu_l + \frac{p}{2}}} = \frac{1 + O(\|\omega\|^{-2})}{1 + O(\|\omega\|^{-2})} = 1 + O(\|\omega\|^{-2}).$$

Furthermore, let $\gamma_l = \sum_{j \neq l} (\nu_j + \frac{p}{2})$, then $p_l(\omega) = O(\|\omega\|^{2\gamma_l})$ where $\gamma_1 > \gamma_2 \cdots > \gamma_L$ and $\gamma_l - \gamma_{l-1} \geq 1$. As a result, the leading term that dominates $\sum_{l=1}^L w_l \sigma_l^2 \alpha_l^{2\nu_l} p_l(\omega)$ is $w_1 \sigma_1^2 \alpha_1^{2\nu_1} p_1(\omega)$, as $\|\omega\| \rightarrow \infty$. Moreover, $\sum_{l=1}^L w_l \sigma_l^2 \alpha_l^{2\nu_l} p_l(\omega) = \|\omega\|^{2\gamma_1} (w_1 \sigma_1^2 \alpha_1^{2\nu_1} + O(\|\omega\|^{-2}))$ since $2\gamma_l - 2\gamma_1 \geq 2, \forall l > 1$.

Now we can analyze the relative difference:

$$\begin{aligned} \left| \frac{\rho(\omega) - \tilde{\rho}(\omega)}{\rho(\omega)} \right| &= \left| \frac{\tilde{\rho}(\omega)}{\rho(\omega)} - 1 \right| = \left| \frac{\sum_{l=1}^L \tilde{w}_l \tilde{\sigma}_l^2 \tilde{\alpha}_l^{2\nu_l} \tilde{p}_l(\omega) \prod_{l=1}^L (\tilde{\alpha}_l^2 + \|\omega\|^2)^{\nu_l + \frac{p}{2}}}{\sum_{l=1}^L w_l \sigma_l^2 \alpha_l^{2\nu_l} p_l(\omega) \prod_{l=1}^L (\alpha_l^2 + \|\omega\|^2)^{\nu_l + \frac{p}{2}}} - 1 \right| \\ &= \left| \frac{\sum_{l=1}^L \tilde{w}_l \tilde{\sigma}_l^2 \tilde{\alpha}_l^{2\nu_l} \tilde{p}_l(\omega)}{\sum_{l=1}^L w_l \sigma_l^2 \alpha_l^{2\nu_l} p_l(\omega)} (1 + O(\|\omega\|^{-2})) - 1 \right| \\ &= \left| \frac{\|\omega\|^{2\gamma_1} (\tilde{w}_1 \tilde{\sigma}_1^2 \tilde{\alpha}_1^{2\nu_1} + O(\|\omega\|^{-2})) (1 + O(\|\omega\|^{-2}))}{\|\omega\|^{2\gamma_1} (w_1 \sigma_1^2 \alpha_1^{2\nu_1} + O(\|\omega\|^{-2}))} - 1 \right| \\ &= \left| \frac{\tilde{w}_1 \tilde{\sigma}_1^2 \tilde{\alpha}_1^{2\nu_1}}{w_1 \sigma_1^2 \alpha_1^{2\nu_1}} (1 + O(\|\omega\|^{-2})) (1 + O(\|\omega\|^{-2})) - 1 \right| \\ &= \left| \frac{\tilde{w}_1 \tilde{\sigma}_1^2 \tilde{\alpha}_1^{2\nu_1}}{w_1 \sigma_1^2 \alpha_1^{2\nu_1}} - 1 + O(\|\omega\|^{-2}) \right|. \end{aligned}$$

As a result, if $w_1 \sigma_1^2 \alpha_1^{2\nu_1} = \tilde{w}_1 \tilde{\sigma}_1^2 \tilde{\alpha}_1^{2\nu_1}$,

$$\int_{\omega \in \mathbb{R}^p: \|\omega\| > 1} \left| \frac{\rho(\omega) - \tilde{\rho}(\omega)}{\rho(\omega)} \right|^2 d\omega \approx \int_{\omega \in \mathbb{R}^p: \|\omega\| > 1} \frac{1}{\|\omega\|^4} d\omega < \infty,$$

when $p = 1, 2, 3$, so $K \equiv \tilde{K}$. That is, none of the parameters are identifiable, while the parameter that might be identifiable is $w_1 \sigma_1^2 \alpha_1^{2\nu_1}$, also known as the microergodic parameter.

Now we turn to the case for $p \geq 5$. By Anderes (2010), it suffices to analyze the principal irregular terms for K . For the spectral density of each individual kernel component, the principal irregular term is

$$G_{\nu_l}(\omega) = \frac{-\pi}{2^{2\nu_l} \sin(\nu_l \pi) \Gamma(\nu_l) \Gamma(\nu_l + 1)} \omega^{2\nu_l} =: C_l \omega^{2\nu_l}.$$

Furthermore,

$$K_l(x + h, x') = \sigma_l^2 G_{\nu_l}(|\alpha_l h|) - \nu_l \sigma_l^2 G_{\nu_l+1}(|\alpha_l h|) + \iota_l(|\alpha_l h|),$$

where $\iota_l(t) = p(|h|) + o(G_{\nu_l+1}(|h|))$ as $|h| \rightarrow 0$ and p is a polynomial with even degree. By linearity, we have

$$\begin{aligned} K(x + h, x') &= \sum_{l=1}^L w_l K_l(x + h, x') \\ &= \sum_{l=1}^L w_l (\sigma_l^2 G_{\nu_l}(|\alpha_l h|) - \nu_l \sigma_l^2 G_{\nu_l+1}(|\alpha_l h|) + \iota_l(t)) \\ &= w_1 \sigma_1^2 G_{\nu_1}(|\alpha_1 h|) - w_1 \nu_1 \sigma_1^2 G_{\nu_1+1}(|\alpha_1 h|) + w_2 \sigma_2^2 G_{\nu_2}(|\alpha_2 h|) + \iota(t), \end{aligned}$$

where $\iota(t) = p(|h|) + o(G_{\nu_2+1}(|h|))$ as $|h| \rightarrow 0$. They by Theorem 4 of Anderes (2010), there exists consistent estimators for $w_1 \sigma_1^2 \alpha_1^{2\nu_1}$ and $w_2 \sigma_2^2 \alpha_2^{2\nu_2} - \nu_1 w_1 \sigma_1^2 \alpha_1^{2(\nu_1+1)}$ when $0 < 2(2\nu_2 - 2\nu_1) < p$, that is $0 < 4 < p$. This completes the proof. \square

C Proof of Corollary 1

We first state a Lemma for comparing MSE of two best linear predictor with two spectral density.

Lemma 3 (Stein (1993)). *Suppose Z is a zero mean stationary process in \mathbb{R}^d and x_1, x_2, \dots is a dense sequence of points in a bounded subset of \mathbb{R}^d . x_0 is a point in the bounded set but not the sequence. Let $\hat{Z}(x_0, n, \rho)$ be the best linear predictor of $Z(x_0)$ based on $Z(x_1), \dots, Z(x_n)$ assuming ρ is the spectral density for Z . $e(x_0, n, \rho) := Z(x_0) - \hat{Z}(x_0, n, \rho)$. If there exists $c > 0$, such that*

$$\lim_{|\omega| \rightarrow \infty} \frac{\rho_1(\omega)}{\rho_0(\omega)} = c$$

and ρ_0 satisfies condition 1 in Lemma 2, then

$$\lim_{n \rightarrow \infty} \frac{\mathbb{E}_{\rho_0} e(x_0, n, \rho_1)^2}{\mathbb{E}_{\rho_0} e(x_0, n, \rho_0)^2} = 1$$

Proof of Corollary 1. For $K_1 = \text{Mat}(w_1 \sigma_1^2, \alpha_1, \nu_1)$, by Theorem 2, $K_1 \equiv K$ since the microergodic parameters match.

Regarding MSE, let ρ be the spectral density of the mixture kernel K , and ρ_1 be the spectral density of the first mixing component K_1 . We assume ρ_1 as the true spectral density. Then by the proof of Theorem 2,

$$\lim_{|\omega| \rightarrow \infty} \frac{\rho(\omega)}{\rho_1(\omega)} = \frac{w_1 \sigma_1^2 \alpha_1^{2\nu_1}}{w_1 \sigma_1^2 \alpha_1^{2\nu_1}} = 1,$$

then the MSE of GP with K_1 is asymptotically equal to the MSE of GP with K . \square

D Proof of Corollary 2

We first state a Lemma regarding the equivalence of Gaussian measure with nuggets.

Lemma 4 (Tang et al. (2022)). *Let S be a closed set, $G_S(m, K)$ denotes the Gaussian measure of the random field on S with mean function m and covariance function K . Let $w(s)$ be a mean square continuous process on S under $G_S(m_1, K_1)$ and χ be a dense sequence of points in S . Then*

1. if $\tau_1^2 \neq \tau_2^2$, then $G_\chi(m_1, K_1, \tau_1^2) \perp G_\chi(m_2, K_2, \tau_2^2)$.
2. if $\tau_1^2 = \tau_2^2$, then $G_\chi(m_1, K_1, \tau_1^2) \equiv G_\chi(m_2, K_2, \tau_2^2)$ if and only if $G_S(m_1, K_1) \equiv G_S(m_2, K_2)$.

Proof of Corollary 2. We denote the adjusted kernel with noise of K and \tilde{K} as K_τ and $\tilde{K}_{\tilde{\tau}}$.

From Lemma 4(1), where we set $m_1 = m_2 = 0$, if $\tau^2 \neq \tilde{\tau}^2$, then $K_\tau \not\equiv \tilde{K}_{\tilde{\tau}}$. If $\tau^2 = \tilde{\tau}^2$, then $K_\tau \equiv \tilde{K}_{\tilde{\tau}}$ if and only if $K \equiv \tilde{K}$. Then the previous results in Theorem 2 holds. \square

E Additional theorem - mixture of Matérn kernels with the same smoothness

Here we introduce a special scenario for Theorem 4 where all component in the mixture kernel have same smoothness. The simulation study for the following theorems are included in Section G: simulation 4.

Theorem 4. *For $K = \sum_{l=1}^L K_l$ where $K_l = \text{Mat}(\sigma_l^2, \alpha_l, \nu)$, then*

- (i) When $p = 1, 2, 3$, the only identifiable parameter is $\sum_{l=1}^L w_l \sigma_l^2 \alpha_l^{2\nu}$.
- (ii) When $p > 4$, the only identifiable parameters are $\sum_{l=1}^L w_l \sigma_l^2 \alpha_l^{2\nu}$ and $\sum_{l=1}^L w_l \sigma_l^2 \alpha_l^{2\nu+2}$.

As a consequence, none of the parameters are identifiable.

Proof. The proof is similar to the proof of Theorem 2. Recall that the spectral densities of K_l are

$$\rho_l(\omega) = \frac{\sigma_l^2 \alpha_l^{2\nu}}{(\alpha_l^2 + \|\omega\|^2)^{\nu + \frac{p}{2}}}, \quad \rho(\omega) = \sum_{l=1}^L w_l \frac{\sigma_l^2 \alpha_l^{2\nu}}{(\alpha_l^2 + \|\omega\|^2)^{\nu + \frac{p}{2}}}, \quad \tilde{\rho}(\omega) = \sum_{l=1}^L \tilde{w}_l \frac{\sigma_l^2 \alpha_l^{2\nu}}{(\alpha_l^2 + \|\omega\|^2)^{\nu + \frac{p}{2}}}.$$

To apply the integral test, first, let $r = 2(\nu + \frac{p}{2})$, then

$$\rho(\omega) \|\omega\|^r = \sum_{l=1}^L w_l \frac{\sigma_l^2 \alpha_l^{2\nu} \|\omega\|^r}{(\alpha_l^2 + \|\omega\|^2)^{\nu + \frac{p}{2}}} \xrightarrow{\omega \rightarrow \infty} \sum_{l=1}^L w_l \sigma_l^2 \alpha_l^{2\nu},$$

that is, bounded away from both 0 and ∞ as $\omega \rightarrow \infty$. Then we check the relative difference between the spectral densities ρ and $\tilde{\rho}$. Observe that

$$\rho(\omega) = \sum_{l=1}^L w_l \frac{\sigma_l^2 \alpha_l^{2\nu}}{(\alpha_l^2 + \|\omega\|^2)^{\nu + \frac{p}{2}}} = \frac{\sum_{l=1}^L w_l \sigma_l^2 \alpha_l^{2\nu} \prod_{j \neq l} (\alpha_j^2 + \|\omega\|^2)^{\nu + \frac{p}{2}}}{\prod_{l=1}^L (\alpha_l^2 + \|\omega\|^2)^{\nu + \frac{p}{2}}} =: \frac{\sum_{l=1}^L w_l \sigma_l^2 \alpha_l^{2\nu} p_l(\omega)}{\prod_{l=1}^L (\alpha_l^2 + \|\omega\|^2)^{\nu + \frac{p}{2}}},$$

where $p_l := \prod_{j \neq l} (\alpha_j^2 + \|\omega\|^2)^{\nu + \frac{p}{2}}$. Observe that

$$|p_l(\omega)| \geq \|\omega\|^{2(L-1)(\nu + \frac{p}{2})} \quad (1)$$

$$\frac{p_l(\omega)}{\|\omega\|^{2(L-1)(\nu + \frac{p}{2})}} = \prod_{j \neq l} \left(1 + \frac{\alpha_j^2}{\|\omega\|^2} \right)^{\nu + \frac{p}{2}} = 1 + O(\|\omega\|^{-2}). \quad (2)$$

Now we can analyze the relative difference:

$$\begin{aligned} \left| \frac{\rho(\omega) - \tilde{\rho}(\omega)}{\rho(\omega)} \right| &= \left| \frac{\frac{\sum_{l=1}^L w_l \sigma_l^2 \alpha_l^{2\nu} p_l(\omega)}{\prod_{l=1}^L (\alpha_l^2 + \|\omega\|^2)^{\nu + \frac{p}{2}}} - \frac{\sum_{l=1}^L \tilde{w}_l \sigma_l^2 \alpha_l^{2\nu} p_l(\omega)}{\prod_{l=1}^L (\alpha_l^2 + \|\omega\|^2)^{\nu + \frac{p}{2}}}}{\frac{\sum_{l=1}^L w_l \sigma_l^2 \alpha_l^{2\nu} p_l(\omega)}{\prod_{l=1}^L (\alpha_l^2 + \|\omega\|^2)^{\nu + \frac{p}{2}}}} \right| \\ &= \left| \frac{\sum_{l=1}^L w_l \sigma_l^2 \alpha_l^{2\nu} p_l(\omega) - \sum_{l=1}^L \tilde{w}_l \sigma_l^2 \alpha_l^{2\nu} p_l(\omega)}{\sum_{l=1}^L w_l \sigma_l^2 \alpha_l^{2\nu} p_l(\omega)} \right| \\ &\leq \frac{1}{\sum_{l=1}^L w_l \sigma_l^2 \alpha_l^{2\nu}} \left| \frac{\sum_{l=1}^L w_l \sigma_l^2 \alpha_l^{2\nu} p_l(\omega) - \sum_{l=1}^L \tilde{w}_l \sigma_l^2 \alpha_l^{2\nu} p_l(\omega)}{\|\omega\|^{2(L-1)(\nu + \frac{p}{2})}} \right| \\ &= \frac{1}{\sum_{l=1}^L w_l \sigma_l^2 \alpha_l^{2\nu}} \left| \sum_{l=1}^L w_l \sigma_l^2 \alpha_l^{2\nu} (1 + O(\|\omega\|^{-2})) - \sum_{l=1}^L \tilde{w}_l \sigma_l^2 \alpha_l^{2\nu} (1 + O(\|\omega\|^{-2})) \right| \\ &= \frac{1}{\sum_{l=1}^L w_l \sigma_l^2 \alpha_l^{2\nu}} \left| \sum_{l=1}^L w_l \sigma_l^2 \alpha_l^{2\nu} - \sum_{l=1}^L \tilde{w}_l \sigma_l^2 \alpha_l^{2\nu} + O(\|\omega\|^{-2}) \right|. \end{aligned}$$

As a result, if $\sum_{l=1}^L w_l \sigma_l^2 \alpha_l^{2\nu} = \sum_{l=1}^L \tilde{w}_l \sigma_l^2 \alpha_l^{2\nu}$,

$$\int_{\omega \in \mathbb{R}^p: \|\omega\| > 1} \left| \frac{\rho(\omega) - \tilde{\rho}(\omega)}{\rho(\omega)} \right|^2 d\omega \approx \int_{\omega \in \mathbb{R}^p: \|\omega\| > 1} \frac{1}{\|\omega^4\|} d\omega < \infty,$$

when $p = 1, 2, 3$, so $K \equiv \tilde{K}$. That is, none of the parameters are identifiable, while the parameter that might be identifiable is $\sum_{l=1}^L w_l \sigma_l^2 \alpha_l^{2\nu}$, also known as the microergodic parameter.

Now we turn to the case for $p \geq 5$. The proof is similar to the proof of Theorem 2: it suffices to analyze the principal irregular terms for K . For the spectral density of each individual kernel component, the principal irregular term is

$$G_\nu(\omega) = \frac{-\pi}{2^{2\nu} \sin(\nu\pi) \Gamma(\nu) \Gamma(\nu + 1)} \omega^{2\nu} =: C_l \omega^{2\nu}.$$

Furthermore,

$$K_l(x + h, x') = \sigma_l^2 G_\nu(|\alpha_l h|) - \nu \sigma_l^2 G_{\nu+1}(|\alpha_l h|) + \iota(|\alpha_l h|),$$

where $\iota(t) = p(|h|) + o(G_{\nu+1}(|h|))$ as $|h| \rightarrow 0$ and p is a polynomial with even degree. By linearity, we have

$$\begin{aligned} K(x+h, x') &= \sum_{l=1}^L w_l K_l(x+h, x') \\ &= \sum_{l=1}^L w_l (\sigma_l^2 G_\nu(|\alpha_l h|) - \nu \sigma_l^2 G_{\nu+1}(|\alpha_l h|) + \iota(t)) \\ &= \sum_{l=1}^L w_l \sigma_l^2 G_\nu(|\alpha_l h|) - \sum_{l=1}^L \nu w_l \sigma_l^2 G_{\nu+1}(|\alpha_l h|) + \iota(t), \end{aligned}$$

where $\iota(t) = p(|h|) + o(G_{\nu+1}(|h|))$ as $|h| \rightarrow 0$. They by Theorem 4 of Anderes (2010), there exists consistent estimators for $\sum_{l=1}^L w_l \sigma_l^2 \alpha_l^{2\nu}$ and $\sum_{l=1}^L w_l \sigma_l^2 \alpha_l^{2(\nu+1)}$ when $0 < 2(2(\nu+1) - 2\nu) < p$, that is $0 < 4 < p$. This completes the proof. \square

F Proof of Theorem 3

(i) is a direct corollary of Theorem 3 of Bachoc et al. (2022), where $\sigma_{ij} \sigma_{jj} \rho_{ij} = A_{ij} \sigma^2$ and $\alpha_{ij} = \frac{1}{\alpha}$ for any $i, j = 1, \dots, m$.

Now we prove (ii). Let θ be the microergodic parameter of K_0 , that is, $K_0 \equiv \tilde{K}_0 \iff \theta = \tilde{\theta}$, where \tilde{K}_0 is characterized by $\tilde{\theta}$. Let ρ_0 and $\tilde{\rho}_0$ be the spectral densities of K and \tilde{K}_0 , then the matrix spectral densities of K and \tilde{K} are $P := A\rho_0$ and $\tilde{P} := \tilde{A}\tilde{\rho}_0$. By the assumption, that is, there exists constants $b, c_1, c_2 > 0$ and $\gamma \in \mathcal{W}_{[-b, b]^m}$ such that $c_1 \gamma^2(\omega) \leq \rho_0(\omega) \leq c_2 \gamma^2(\omega)$, we claim that there exists $q_1, q_2 > 0$ such that

$$q_1 \gamma^2(\omega) \mathbf{I}_m \leq P(\omega) \leq q_2 \gamma^2(\omega) \mathbf{I}_m, \quad \forall \omega \in \mathbb{R}^p. \quad (3)$$

From the assumption,

$$P(\omega) = A\rho_0 \leq c_2 \gamma^2(\omega) A \leq c_2 \text{eig}_1(A) \gamma^2(\omega),$$

where $\text{eig}_1(A)$ is the largest eigenvalue of A . Similarly, $c_1 \text{eig}_m(A) \gamma^2(\omega) \mathbf{I}_m \leq P(\omega)$ where $\text{eig}_m(A) > 0$ is the smallest eigenvalue of A , which is positive by the positive definiteness of A . Then claim (3) holds where $q_1 := c_1 \text{eig}_m(A)$ and $q_2 := c_2 \text{eig}_1(A)$. Now we can prove (ii). If $\theta A = \tilde{\theta} \tilde{A}$, then for any $i, j = 1, \dots, m$,

$$\begin{aligned} \int_{\mathbb{R}^p} \frac{1}{\gamma^4(\omega)} \left(P_{ij}(\omega) - \tilde{P}_{ij}(\omega) \right)^2 d\omega &= \int_{\mathbb{R}^p} \frac{1}{\gamma^4(\omega)} \left(A_{ij} \rho_0(\omega) - \tilde{A}_{ij} \tilde{\rho}_0(\omega) \right)^2 d\omega \\ &= \int_{\mathbb{R}^p} \frac{1}{\gamma^4(\omega)} \left(\theta A_{ij} \frac{\rho_0(\omega)}{\theta} - \tilde{\theta} \tilde{A}_{ij} \frac{\tilde{\rho}_0(\omega)}{\tilde{\theta}} \right)^2 d\omega \\ &= \int_{\mathbb{R}^p} \frac{1}{\gamma^4(\omega)} \left(\theta A_{ij} \frac{\rho_0(\omega)}{\theta} - \theta A_{ij} \frac{\tilde{\rho}_0(\omega)}{\tilde{\theta}} \right)^2 d\omega \\ &= (\theta A_{ij})^2 \int_{\mathbb{R}^p} \frac{1}{\gamma^4(\omega)} \left(\frac{\rho_0(\omega)}{\theta} - \frac{\tilde{\rho}_0(\omega)}{\tilde{\theta}} \right)^2 d\omega \\ &< \infty, \end{aligned}$$

where the last inequality holds from the assumption that θ is the microergodic parameter of K_0 . As a result, by Theorem 2 of Bachoc et al. (2022), θA is the microergodic parameter of K .

G Experiment details

G.1 Simulation 1

In the first simulation, we examined a mixture kernel defined as follows: $K = \sum_{l=1}^3 w_l K_l$, wherein K_l represents the Matérn kernel with parameters $(\sigma_l^2, \alpha_l, \nu_l)$. For this simulation, we assigned the values $\nu_1 = 1/2, \nu_2 = 3/2, \nu_3 = 5/2$ for the smoothness parameter.

The weights for each kernel component, represented as (w_1, w_2, w_3) , were chosen as $(0.03, 0.33, 0.63)$. This set-up presents the case where despite w_1 being the smallest, which is associated with the kernel that exhibits the least smoothness, our result further substantiates our claim about the dominance of the kernel with the lowest smoothness over the influence of weights. In terms of the scale parameters, for $(\sigma_1^2, \sigma_2^2, \sigma_3^2)$, we picked $(3, 3, 3)$. We selected $(\alpha_1, \alpha_2, \alpha_3)$ to be $(1, 1, 1)$. This uniform selection across the components aids in isolating the effect of the smoothness and weights in our analysis.

G.2 Simulation 2

In the second simulation, we consider the following mixture kernel: $K = \sum_{l=1}^3 w_l K_l$, where K_l is the Matérn kernel with parameter $(\sigma_l^2, \alpha_l, \nu_l)$. For this simulation, the values for the smoothness parameter, ν , were set as $\nu_1 = 1/2, \nu_2 = 3/2, \nu_3 = 5/2$. Regarding the choice of the weight parameters (w_1, w_2, w_3) , we selected $(0.1, 0.3, 0.6)$ to reflect the difference in contribution of each kernel to the overall mixture. Although the weight of the Matérn $1/2$ kernel (w_1) is small, it still remains dominant due to its lesser smoothness. This setup allowed us to test our hypothesis that smoothness plays a more significant role than weight in determining the identifiability of parameters. $(\sigma_1^2, \sigma_2^2, \sigma_3^2)$ are set to $(16, 4, 1)$, and $(\alpha_1, \alpha_2, \alpha_3)$ are set to $(4, 2, 1)$. This variation further facilitated the examination of our proposition that the parameters associated with the least smooth kernel converge to their true values, while others do not.

In this scenario, we generate $X \in \mathbb{R}^2$ from an equal-spaced sequence ranging from -10 to 10 , with a random variation sampled from $\text{unif}(-\frac{1}{5n}, \frac{1}{5n})$. The sample size, n , takes on values from the set $20, 50, 100, 500$. For each sample size, we replicate the simulation 100 times. Subsequently, Y is simulated from $N(0, K + \epsilon)$. We consider ϵ as a fixed value ($\epsilon = 0.1$) and include it for numerical robustness. This ϵ is also added in the training process. For parameter initialization, we initialize $w = (0.2, 0.3, 0.5)$, $\sigma^2 = (5.0067, 10, 15)$ and $\alpha = (0.7615, 0.4702, 0.3280)$. These initial values were close to the true parameters, yet sufficiently distinct to illustrate the efficacy of the learning process. Here we use the SGD optimizer with 0.005 learning rate and 1000 epochs. All parameter estimates are summarised in the Figure S1.

We further examined the simulation in a larger sample size and also used a different optimizer L-BFGS (learning rate 0.5 for $n = 50, 500, 1.0$ for $n = 100$). The results are consistent with the previous results.

G.3 Simulation 3

In the third simulation, we consider the following mixture kernel: $K = AK_0$, where K_0 is the Matérn kernel with parameter (α, σ^2, ν) . For this simulation, we set $\nu = 1/2$. The ground truth for the parameters is assigned as follows: the matrix A is set as $[[5, 1][1, 5]]$, which serves as a symmetric, positive-definite structure to facilitate the properties of the covariance matrix; σ^2 is set to 10, and α is set to 1.

In this simulation, we generate $X \in \mathbb{R}^2$ from an equal-spaced sequence ranging from -10 to 10 , with a random variation sampled from $\text{unif}(-\frac{1}{5n}, \frac{1}{5n})$. The sample size, n , takes on values from the set $50, 100, 200, 400$. For each sample size, we replicate the simulation 100 times. Subsequently, Y is simulated from $N(0, K + \epsilon)$. We consider ϵ as a fixed value ($\epsilon = 0.5$). This ϵ is also added in the training process. In terms of parameter initialization, we elect to start with A as an identity matrix, $\sigma^2 = 1$ and $\alpha = 10$. The initialization of A as an identity matrix ensures a simple, non-informative starting point, while the initial σ^2 and α are chosen to be significantly distinct from the ground truth to assess the robustness of the learning process. Here we use the SGD optimizer with 0.001 learning rate and 2000 epochs. The parameter estimates of A are summarised in the Figure S4.

G.4 Additional simulation (Simulation 4) for mixture of Matérn kernels with the same smoothness

In this additional simulation 4, we aim to evaluate the parameter identifiability in a GP with a mixture kernel consisting of Matérn kernels with the same smoothness. We denote the mixture as $K = \sum_{l=1}^L w_l K_l$, where K_l is a Matérn kernel with parameters $(\sigma_l^2, \alpha_l, \nu)$. Our theorem suggests that only the microergodic parameter $\sum_{l=1}^L w_l \sigma_l^2 \alpha_l$ might be identifiable, while other parameters are

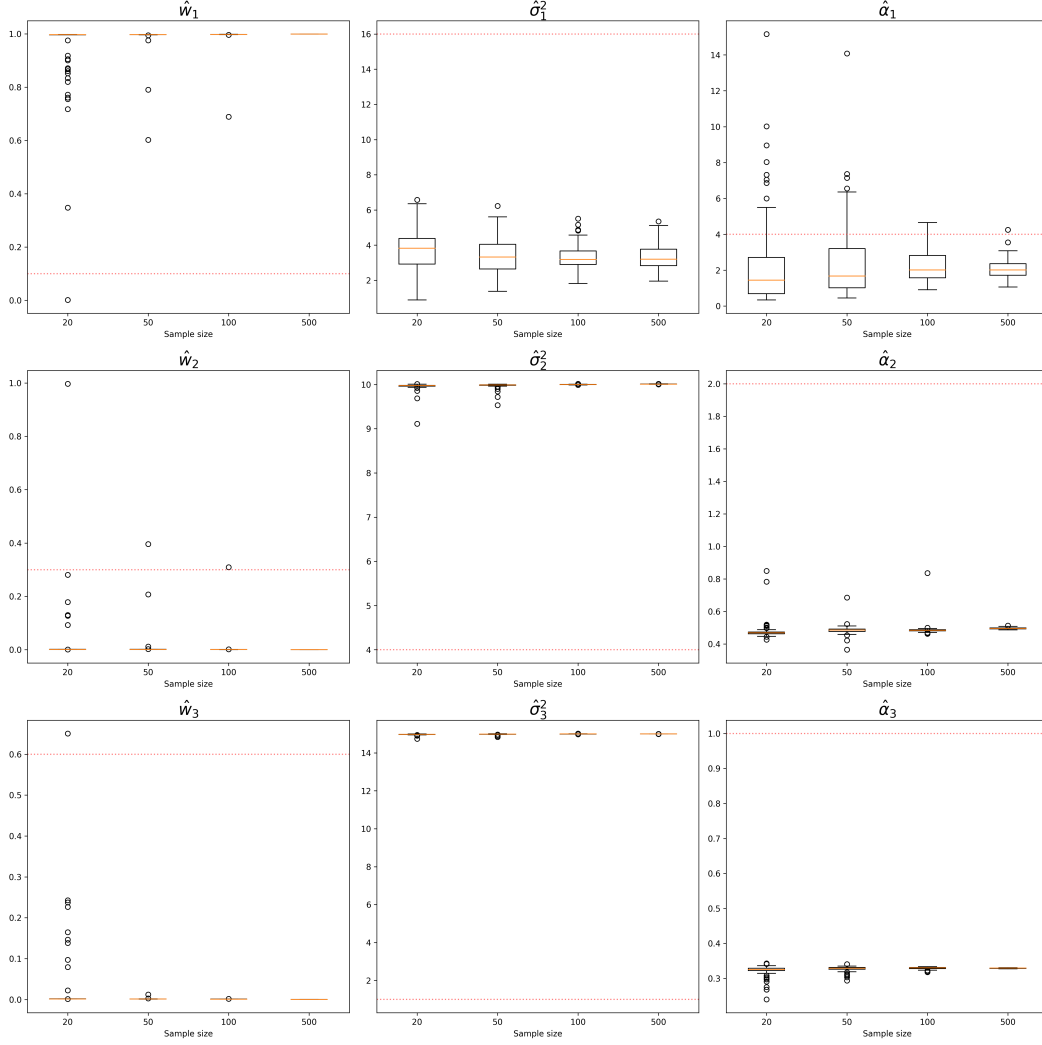


Figure S1: All parameter estimation in simulation 2.

not identifiable. Consequently, we will evaluate the parameter estimation by comparing it with the true value for different training sample sizes.

Here we use mixture of three Matérn 1/2 kernels. We generate $X \in \mathbb{R}^2$ from an equal-spaced sequence with values ranging from -10 to 10 , with a random variation sampled from $\text{unif}(-\frac{1}{10n}, \frac{1}{10n})$. The sample size n takes values from 20, 50, 100, 500. For each sample size, we replicate the simulation 100 times. Subsequently, we simulate Y from a normal distribution with a mean of 0 and covariance matrix $K + \epsilon$. We treat ϵ as a fixed value ($\epsilon = 0.1$) and include it for numerical robustness. This ϵ is also added in the training process. The ground truth parameters are given as $w = (0.2, 0.3, 0.5)$, $\sigma^2 = (16, 4, 1)$ and $\alpha = (2, 1, 4)$. Here the weight and sigma are set to true value, $(\alpha_1, \alpha_2, \alpha_3)$ are set to $(4, 2, 1)$. The motivation behind our specific parameter initialization strategy is to intentionally introduce some degree of initial discrepancy. This approach allows us to critically observe the convergence behavior of the parameters. Here we use the Adam optimizer with 0.01 learning rate and 1000 epochs.

Our results offer compelling evidence that, in the case of a mixture kernel consisting of three Matérn 1/2 kernels, only the MLE of the microergodic parameter $\sum_{l=1}^L w_l \sigma_l^2 \alpha_l^{2\nu}$ converges to the true value (Figure S5A). The MLEs of all other parameters do not demonstrate convergence to their corresponding true values (Figure S5B-D). This result underscores the importance of understanding the

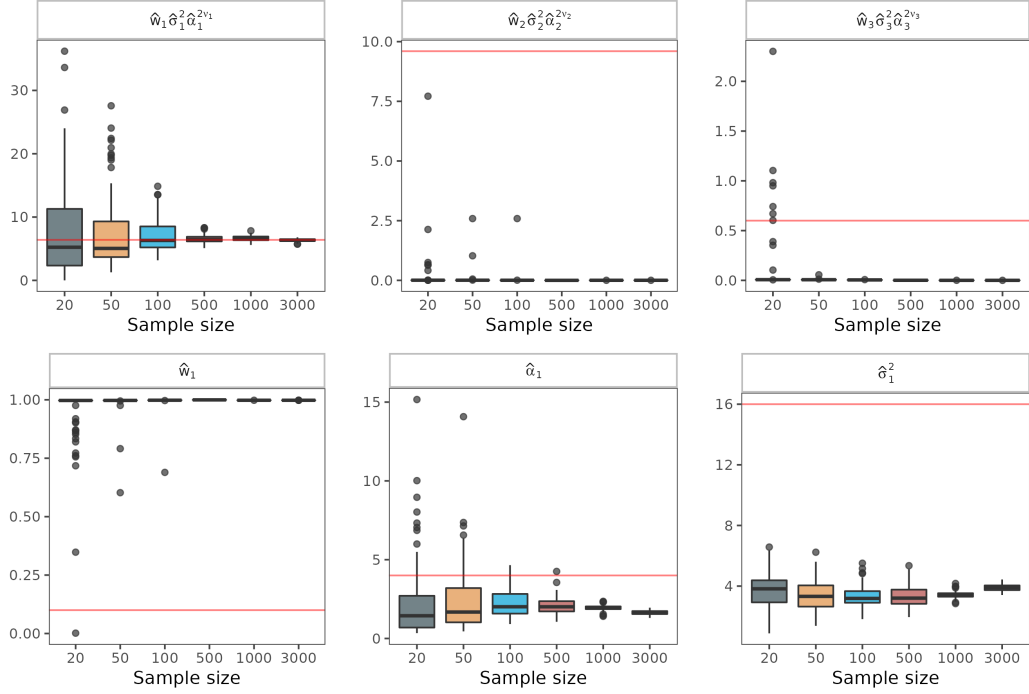


Figure S2: Parameter estimation in simulation 2 with larger sample size.

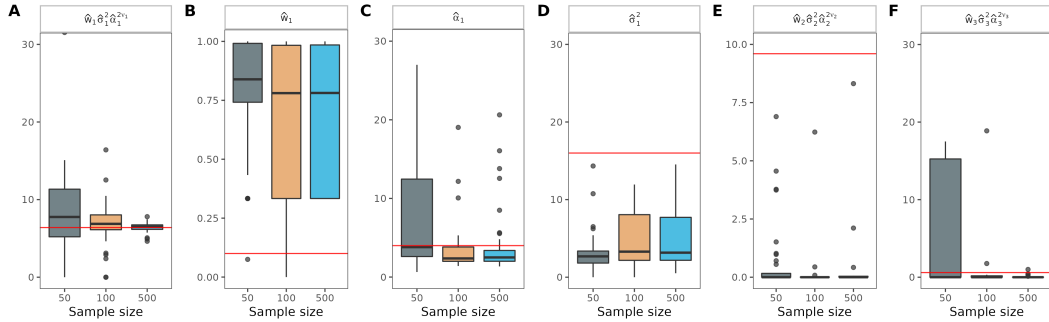


Figure S3: Parameter estimation in simulation 2 with L-BFGS optimizer.

identifiability of parameters in such mixture kernels and highlights the need for careful consideration when interpreting the estimated parameters in Gaussian process models. When treating mixture kernel consist of same smoothness, we could not interpret every single model. All parameter estimates are summarised in Figure S6.

G.5 Application 1

In application 1, we focus on image analysis. We employ a hand-written zero from the MNIST dataset (LeCun et al. (1998)). In this application, we use mixture kernel with Matérn kernels of smoothness $1/2$, $3/2$ and $5/2$ and compare its performance with Matérn $1/2$ kernel. For both kernels, we used the SGD optimizer with learning rate $1e^{-05}$. The training epochs are 40000. During both the training and prediction stages, we introduced a term, ϵ , into the covariance computation to guarantee its positive-definiteness. For both kernels, we set ϵ to 0.01. For mixture kernel, the parameters are initialized as $(w_1, w_2, w_3) = (1/3, 1/3, 1/3)$, $(\sigma_1^2, \sigma_2^2, \sigma_3^2) = (1, 1, 1)$ and $(\alpha_1, \alpha_2, \alpha_3) = (1, 1, 1)$.

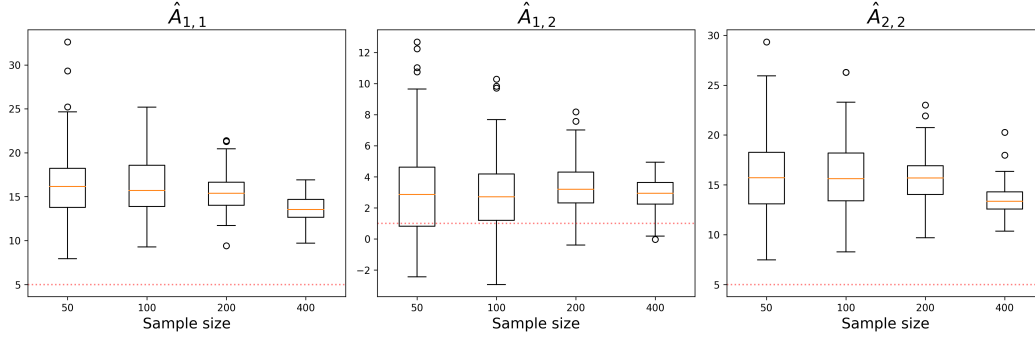


Figure S4: Parameter estimation in simulation 3.

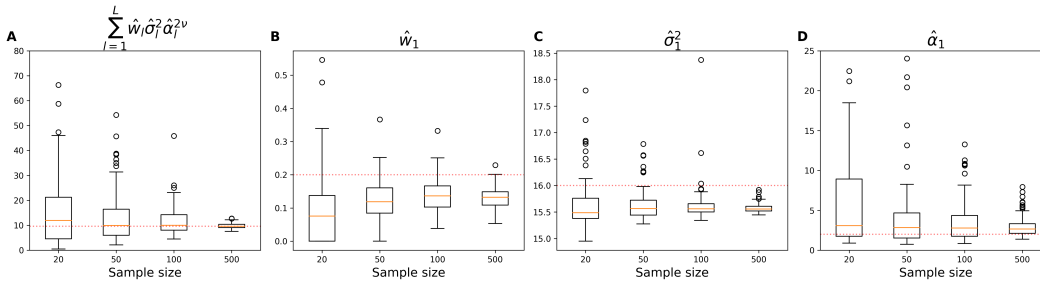


Figure S5: Parameter estimation in simulation 4. (A) Only the microergodic parameter $\sum_{l=1}^L w_l \sigma_l^2 \alpha_l$ might be identifiable (B-D) All other parameters $(\sigma_l^2, \alpha_l, w_l)_{l=1}^L$ are not identifiable.

Here the estimated parameters for mixture kernel are $(w_1, w_2, w_3) = (9.9954e^{-01}, 2.3194e^{-04}, 2.3194e^{-04})$, $(\sigma_1^2, \sigma_2^2, \sigma_3^2) = (1.2148e^{+02}, 4.9960e^{+01}, 4.9256e^{+01})$, $(\alpha_1, \alpha_2, \alpha_3) = (1.3941e^{-01}, 1.1203e^{-02}, 1.1020e^{-02})$. The estimated parameters for Matérn 1/2 kernel are $\alpha = 3.0639e^{-02}, \sigma^2 = 2.7927e^{+02}$.

G.6 Application 2

In application 2, we focus on the Moana Loa CO₂ dataset (Tans and Keeling (2023)). In this application, we compare the performance of Matérn mixture 1/2 + 3/2, 1/2 + 3/2 + 5/2, 3/2 + 5/2 and three single Matérn kernels (1/2, 3/2, 5/2). We use sklearn package (Pedregosa et al. (2011)) for this analysis. The parameters are initialized as $(\sigma_1^2, \sigma_2^2, \sigma_3^2) = (10, 500, 500)$ and $(\alpha_1, \alpha_2, \alpha_3) = (4, 0.1, 0.1)$ for both single kernel and mixture kernel. Other parameters remain default in sklearn.

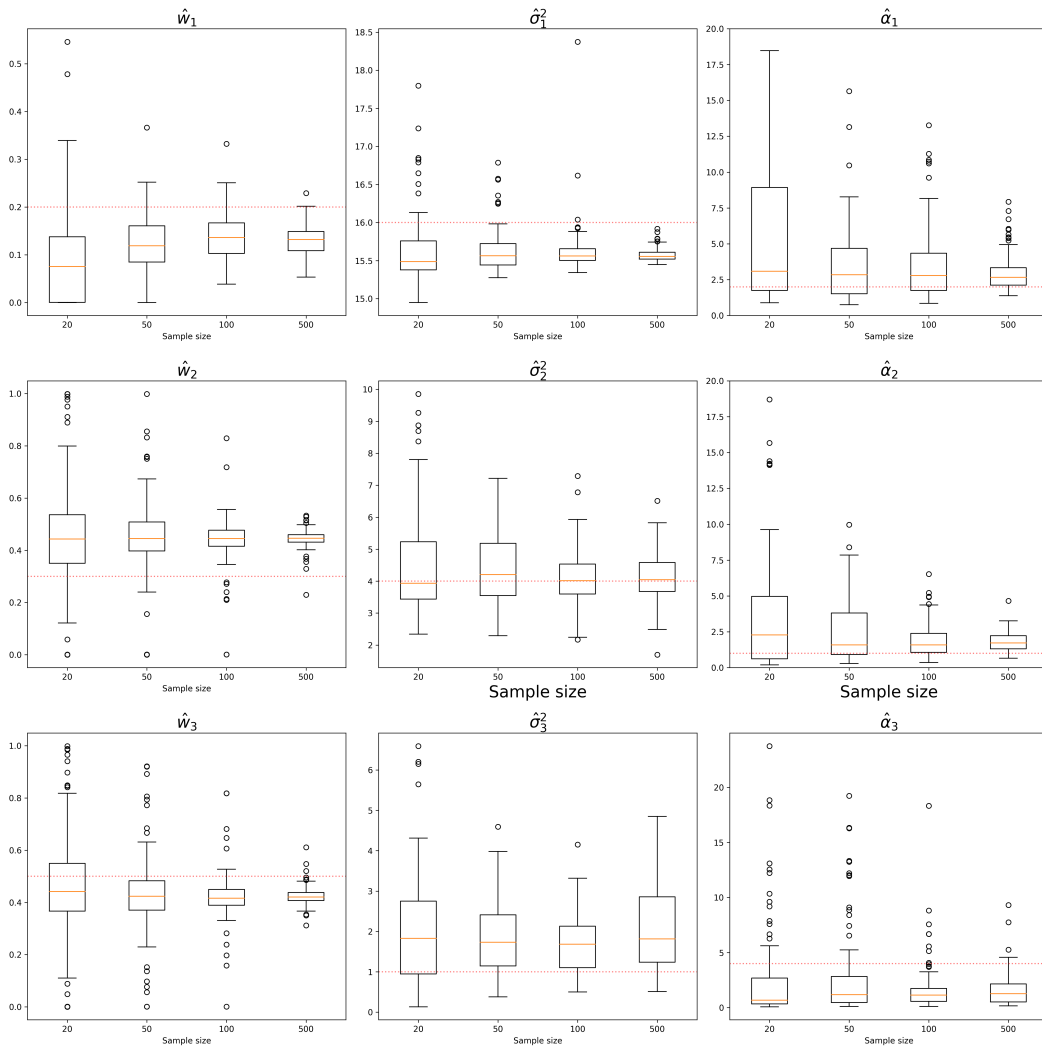


Figure S6: All parameter estimation in simulation 4.